BMC Veterinary Research

RESEARCH

Open Access

Efficacy and mechanism of action of harmine derivative H-2-104 against *Echinococcus granulosus* infection in mice

Huijing Gao[1,2†], Qinwei Xu[1,3†], Jiang Zhu[2,5†], Kadierya Kuerban[1,4], Bei Chen[1], Jun Zhao[1], Kalibixiati Aimulajiang[2,6*] and Liang Teng[1,2*]

Abstract

Background Cystic echinococcosis (CE) is a chronic zoonotic parasitic disease caused by the parasite *Echinococcus granulosus* (*E. granulosus*). Currently, pharmacologic treatments are limited to albendazole and mebendazole; however, these treatments are associated with significant side effects and limited therapeutic efficacy, highlighting the urgent need for the development of new drugs. Harmine (HM) has been reported to exhibit potent antiparasitic effects, although it is also accompanied by notable neurotoxicity. H-2-104, a derivative of HM obtained through structural modification of its parent nucleus, represents a promising candidate for further investigation. This study aims to assess the in vivo and in vitro efficacy of H-2-104 against *E. granulosus* and to elucidate the mechanism of action of H-2-104 against CE from a metabolomics perspective.

Methods In vitro pharmacodynamics experiments were conducted to assess the inhibitory activity of H-2-104 against *E. granulosus* protoscoleces (PSCs). Following this, a mouse model of *E. granulosus* infection was established to explore the inhibitory effects against *E. granulosus* of H-2-104 at low, medium, and high concentrations. Additionally, non-targeted metabolomic approaches were utilized to analyze the serum and liver samples from mice in the control group, model group, and H-2-104 treatment group with the aim of identifying relevant biomarkers and crucial metabolic pathways involved in the response to H-2-104 treatment.

Results The in vitro results demonstrated that H-2-104 exhibited significantly superior inhibitory activity against PSCs compared to harmine and albendazole. Morphological observations revealed marked alterations in the ultrastructural characteristics of PSCs treated with H-2-104. In vivo pharmacodynamic studies showed that H-2-104 at a dosage of 100 mg/kg exhibited the highest cyst inhibition rate, which was (73.60 ± 4.71)%. Metabolomics analysis revealed that 64 serum metabolites were significantly altered, primarily involving metabolic pathways such as necroptosis, linoleic acid metabolism, and phenylalanine metabolism. Additionally, 81 liver metabolites were identified with significant

†Huijing Gao, Qinwei Xu and Jiang Zhu contributed equally to this work.

*Correspondence:
Kalibixiati Aimulajiang
kali0920@163.com
Liang Teng
tl750212@126.com

Full list of author information is available at the end of the article

differences, mainly involving metabolic pathways like fructose and mannose metabolism, and glycerophospholipid metabolism.

Conclusions H-2-104 exhibits significant activity both in vitro and in vivo, suggesting its potential as a promising new drug for the treatment of CE. The anti-CE effects of H-2-104 may be attributed to its regulation of multiple biological pathways, including cell apoptosis, amino acid metabolism, and glucose metabolism.

Graphical Abstract

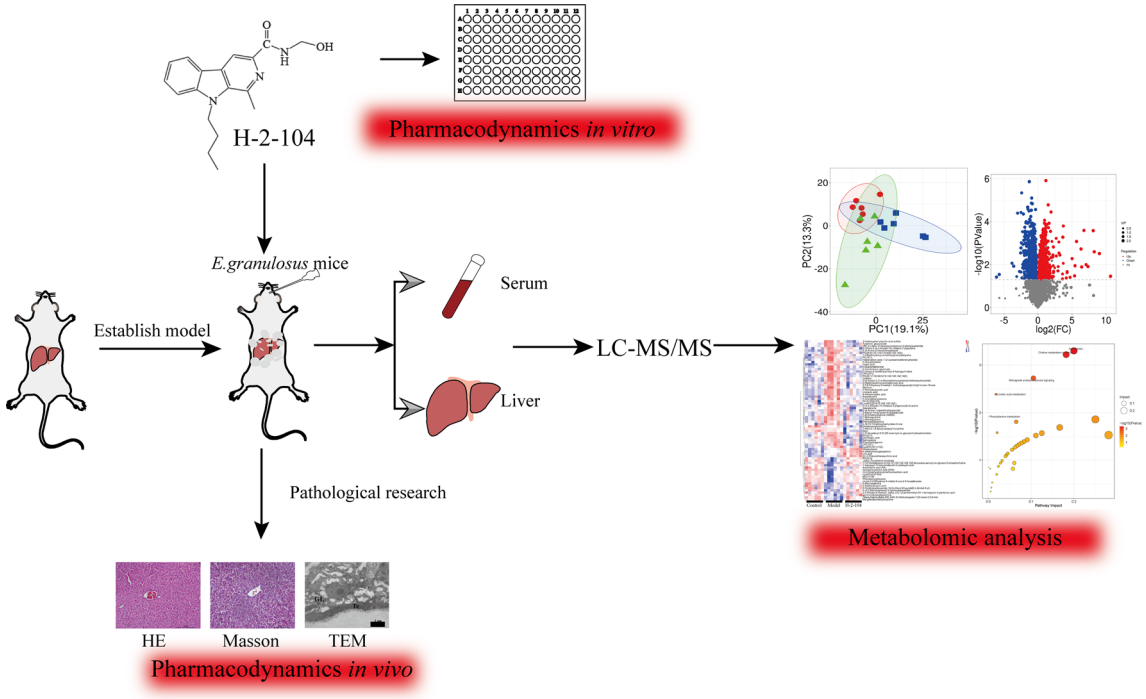

Keywords Cystic echinococcosis, *Echinococcus granulosus;* Harmine derivative, UPLC-MS/MS, Metabolomics, Metabolites

Introduction

Cystic echinococcosis (CE) is a severe zoonotic parasitic disease caused by the larval stage of the tapeworm *Echinococcus granulosus*(*E. granulosus*) parasites in humans or animals [1–3], and it is classified as one of the most serious parasitic diseases in humans by the World Health Organization (WHO) and the Food and Agriculture Organization of the United Nations (FAO) [4]. This disease is predominantly distributed in regions with developed animal husbandry [5]. In China, CE is predominantly prevalent in pastoral and semi-pastoral areas of seven provinces and autonomous regions, namely Nei Mongol, Sichuan, Tibet, Gansu, Qinghai, Ningxia, and Xinjiang [6]. According to statistics, the direct economic loss in western China due to echinococcosis amounts to RMB 3 billion yuan annually [7, 8]. CE has been listed by the World Health Organization as one of 17 neglected diseases that need to be controlled or eliminated by 2050 [9, 10].The infection caused by *E. granulosus* primarily affects organs with rich blood supply, with the liver being the most common site [11]. The presence of occupational lesions at the site of *E. granulosus* infection leads to discomfort, and such infections impact the structure and function of the liver, primarily disrupting its metabolic, detoxifying, and excretory capabilities. Additionally, there is a risk of secondary infections, which collectively impairs the patient's quality of life [12].

Currently, the treatment options for CE primarily encompass surgical intervention and pharmacological therapy [13]. Surgical procedures are primarily indicated for patients with definitive surgical indications, whereas pharmacological therapy represents the sole approach for those ineligible for surgery [14]. Albendazole (ABZ), belonging to the benzimidazole class of drugs, is currently the first-line clinical treatment for CE and is also one of the drugs recommended by the WHO for the

management of CE [15]. Despite its widespread use in the treatment of CE, ABZ exhibits poor solubility, leading to inadequate absorption after oral administration, and low drug concentrations in plasma and liver, and thus, only about one-third of patients achieve remission or cure [16, 17]. 20~40% of patients exhibit suboptimal treatment outcomes. Furthermore, ABZ acts to inhibit rather than expel the parasite, necessitating long-term administration [18], which in turn predisposes patients to adverse reactions such as nausea, vomiting, alopecia, renal impairment, mucosal damage, and even death [19]. Consequently, it is urgent to develop novel and effective chemotherapeutic agents. Recent years have witnessed remarkable advancements in pharmacological research targeting *Echinococcus granulosus* infections, with particular emphasis on the identification of bioactive plant-derived compounds exhibiting anthelmintic properties from traditional medicinal botanicals. Notably, systematic phytochemical investigations have validated the therapeutic potential of several species including Zataria multiflora [20, 21], Nigella sativa [22], Berberis vulgaris [23], Allium sativum [24, 25] and crocin [26, 27]. These findings not only corroborate the empirical knowledge of traditional healing systems but also lay the foundation for substantial progress in developing novel anti-echinococcosis therapeutics through modern pharmaceutical approaches.

Peganum harmala L., a perennial herb belonging to the *Zygophyllaceae* family, has been traditionally used as a medicinal herb by ethnic groups such as Uyghurs, Kazaks, and Mongolians [28, 29]. *Peganum harmala L.* contains a variety of chemical compositions, such as alkaloids, flavonoids, anthraquinones, triterpenoids, steroids, phenolic glycosides and volatile oils, etc., of which alkaloids are the most abundant, up to 2 ~ 6 %. Alkaloids mainly include β-carbolines and quinolines, and the most researched alkaloid is harmine among the β-carboline alkaloids [30]. The medicinal parts include its seeds and whole plant, with the major chemical constituent being harmine (HM) (Fig. 1A). Numerous studies have reported that HM exhibits a wide range of pharmacological activities, including antibacterial [31], antiparasitic [32–36], antitumor [37–40], antidepressant [41–44], and antidiabetic effects [45]. Our research team has discovered that HM possesses significant anti-CE activity [46]. However, studies have also shown that HM has strong neurotoxicity, capable of stimulating the central nervous system and causing adverse reactions or even life-threatening conditions in humans and animals, thereby limiting its clinical application [47]. To reduce the neurotoxicity of HM, our research group previously conducted structural modification on HM to obtain the derivative H-2-104 (Fig. 1B). Preliminary studies have indicated that H-2-104 exhibits favorable absorption properties and high bioavailability [48], suggesting that H-2-104 may be a potential therapeutic agent for CE and warrants further in-depth investigation.

Metabolomics, an emerging discipline developed in recent years, involves the analysis of metabolites within organisms to observe changes in metabolites under different physiological or pathological states, thereby elucidating the relationships between metabolites and their corresponding physiological or pathological conditions. Currently, metabolomics is widely applied in various fields such as drug discovery and development, disease diagnosis, therapeutic efficacy assessment, toxicological evaluation, and biomarker discovery [49–51].

In this study, we first investigated the inhibition of *E. granulosus* activity of H-2-104 through in vitro and in vivo pharmacodynamics experiments. Subsequently, based on LC-MS/MS technology, we detected changes in serum and liver metabolites in mice infected with *E. granulosus* after the intervention, identified potential biomarkers and the involved metabolic pathways, and explored the mechanism of action of H-2-104 against CE.

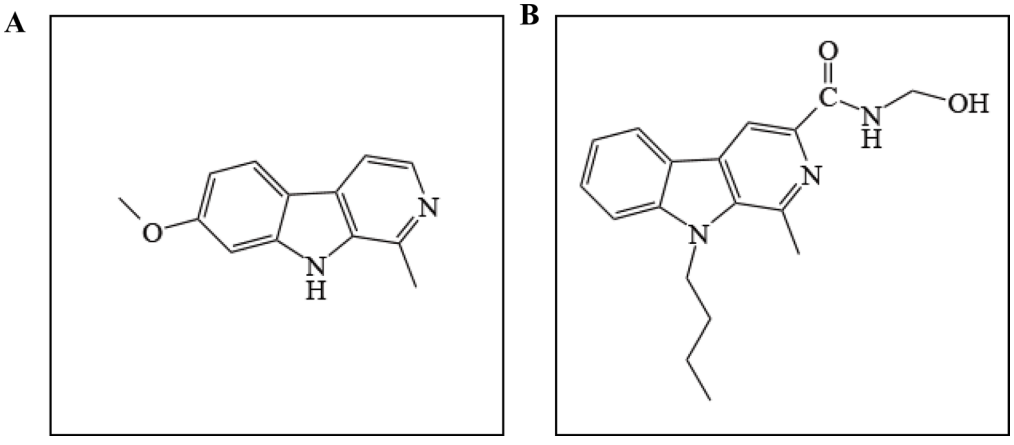

Fig. 1 The molecular structures of harmine (**A**) and harmine derivatives H-2-104 (**B**)

Our findings provide a potentially valuable reference for the development of anti-CE drugs.

Materials and methods

Chemicals and reagents

ABZ (purity > 98%) was purchased from Sigma-Aldrich (St. Louis, USA). HM and H-2-104 (purity > 98%) were synthesized by Xinjiang Huashidan Pharmaceutical Co., Ltd. Unless stated otherwise, all culture reagents were purchased from Gibco (Wisent, Canada).

Animals

Eighty female Kunming(KM) mice, aged 6–8 weeks, of Specific Pathogen Free grade with a body weight of 20 ± 2 g, were purchased from the Experimental Animal Center of Xinjiang Medical University. The experimental animal production license number is SYXK (Xin) 2018-0003 The animals were housed in a barrier environment at the Animal Experimentation Center of Xinjiang Medical University. China. This experiment was approved by the Experimental Animal Ethics Committee of Xinjiang Medical University with the approval number: IACUC-20170420-04.

Parasites collection and culture

Protoscoleces (PSCs) were isolated from hepatic cysts of naturally infected sheep slaughtered at the Hualing Slaughterhouse in Urumqi, Xinjiang. The method for collecting and culturing PSCs refers to previous studies [33]. Briefly, cyst fluid was aspirated from the hepatic cysts, and after natural sedimentation, the supernatant was discarded to collect the PSCs. The PSCs were washed five times with sterile saline and then digested with 1% pepsin (pH = 2.0) for 30 min. After filtration through a sieve, they were washed with saline-containing antibiotics until the viability of the PSCs reached over 98% [52]. Subsequently, the PSCs were transferred to a 25 cm^2 cell culture flask containing RPMI 1640 medium supplemented with 2% penicillin (100 U/mL) and streptomycin (100 μg/mL), and 10% fetal bovine serum. The viability of the PSCs was assessed using 1% eosin staining, with a requirement of greater than 95% viability. The eligible PSCs were then cultured in an incubator at 37 °C with 5% CO_2.

Effect of H-2-104 on PSCs in vitro

PSCs were subjected to adaptive culturing for 48 h, and their viability was assessed. PSCs with viability greater than 95% were added to a 96-well plate, with approximately 200 PSCs per well. 0.1% dimethyl sulfoxide (DMSO, Amresco, USA) group was used as the negative control; The HM and H-2-104 groups were dissolved in DMSO and 2 μL was added to wells to make the final concentrations of 6.25, 12.5, 25, 50, 100 and 200 μM, respectively. PSCs were collected at 1, 2, 3, 4, and 5 days, respectively.The survival rate of PSCs in each group was detected by eosin staining method. The experiment was performed in triplicate. Additionally, changes in the ultrastructure of PSCs were also observed using a scanning electron microscope (SEM) (JSM-6390LV, JEOL Ltd., Tokyo, Japan).

Subacute toxicity study of H-2-104 in mice

The subacute toxicity study in mice was performed according to OECD Guideline No. 407 [53]. Fifty KM mice were randomly divided into five groups of ten animals each (five female and five male): (1) control group, given 0.5% CMC-Na; (2)HM group, given 100 mg/kg/day HM suspension; (3) H-2-104 groups (low, medium and high), given 50, 100 or 200 mg/kg/day H-2-104 suspension. After 30 days of intragastric administration, blood was collected from anesthetized mice. The biochemical parameters were measured, and liver, kidney and brain tissues were collected for pathological examination.

Effect of H-2-104 on *E. granulosus*-infected mice in vivo

A 0.2 mL suspension of normal saline containing 3000 PSCs was injected into mice via intraperitoneal injection [54]. 8 months after infection, mice successfully infected were randomly divided into five groups (6 mice/group): (1)control group and model group, 0.5% carboxymethyl cellulose (CMC-Na) solution; (2) positive drug group, given 50 mg/kg/day ABZ in 0.5% CMC-Na solution; (3) H-2-104 groups (low, medium and high), given 25, 50 or 100 mg/kg/day H-2-104 in distilled water. Oral administration was carried out for 30 days [13, 18]. At the end of treatment, all animals were anesthetized with isoflurane to collect blood, and euthanized by cervical dislocation to prevent pain. Then the mice were dissected to isolate the livers and cysts, and the cyst inhibition rate was calculated as follows: [(mean cysts weight of the model group) - (mean cysts weight of the intervention group)] / (mean cysts weight of the model group) × 100%. Additionally, cysts were observed by transmission electron microscopy (TEM) (JEM1230, JEOL company, Japan) as described previously; and the liver tissues were collected for histopathological observation. Furthermore, metabolomic analysis was conducted on the liver tissues.

Metabolomics analysis

100 μL of serum was placed in a clean EP tube, and 400 μL of extraction solution containing isotope-labeled internal standards (methanol: acetonitrile, 1:1 (v/v)) were added. The mixture was vortexed for 30 s and then sonicated in an ice-water bath for 10 min. After allowing the sample to stand at -40 °C for an hour, it was centrifuged at 13,800 × *g* for 15 min at 4 °C. The supernatant was transferred to a clean sample vial for analysis. Additionally,

25 mg of liver tissue sample were weighed into a clean EP tube, and homogenization beads were added. 500 µL of extraction solution containing isotope-labeled internal standards (methanol: acetonitrile: water; 2:2:1(v/v/v)) were then added, and the mixture was vortexed for 30 s. The sample was homogenized in a homogenizer (JXFST-PRP-24, shanghaijingye, Shanghai, China) at 35 Hz for four minutes and then transferred to an ice-water bath for five minutes of sonication. This homogenization step was repeated three times. Following this, the sample was incubated at -40 °C for an hour and then centrifuged at 13,800 × *g* for 15 min at 4 °C. The supernatant was transferred to a clean sample vial for analysis.

LC-MS/MS analyses were performed using a high-performance liquid chromatography (HPLC) system (Vanquish, Thermo Fisher Scientific, Waltham, USA, and Bruker BioSpin, Karlsruhe, Germany). The injection volume of the plasma and liver was 2 µL. Data were acquired using an Orbitrap Exploris 120 mass spectrometer (Thermo Fisher Scientific, Waltham, USA, and Bruker BioSpin, Karlsruhe, Germany). Equipped with an electrospray ionization (ESI) source, operating in both positive and negative ion modes. The spray voltage was set to 3.8 kV for positive ions and – 3.4 kV for negative ions. The sheath gas flow rate was 50 arb, and the auxiliary gas flow rate was 15 arb. The capillary temperature was maintained at 320℃. The first-stage resolution was set to 60,000, and the second-stage resolution was set to 15,000.

The raw data were converted to the mzXML format using ProteoWizard and processed with an in-house program, which was developed using R and based on XCMS, for peak detection, extraction, alignment, and integration. The metabolites were identified by accuracy mass and MS/MS data which were matched with HMDB (http://www.hmdb.ca) [55], massbank (http://www.massbank.jp/) [56], KEGG (https://www.genome.jp/kegg/) [57], LipidMaps (http://www.lipidmaps.org) [58], mzcloud (https://www.mzcloud.org) [59] and the metabolite database bulid by Panomix Biomedical Tech Co., Ltd. (Suzhou, China). Two different multivariate statistical analysis models, unsupervised and supervised, were applied to discriminate the groups (PCA; PLS-DA; OPLS-DA) by R ropls (v1.22.0) package [60]. The statistical significance of *P* value was obtained by statistical test between groups. Finally, combined with *P* value, VIP (OPLS-DA variable projection importance) and FC (multiple of difference between groups) to screen biomarker metabolites. By default, when $P < 0.05$ and VIP > 1, we think that metabolite were considered to have significant differential expression. Differential metabolites were subjected to pathway analysis by MetaboAnalyst [61], which combines results from powerful pathway enrichment analysis with the pathway topology analysis. The identified metabolites in metabolomics were then mapped to the KEGG pathway for biological interpretation of higher-level systemic functions. The metabolites and corresponding pathways were visualized using KEGG Mapper tool. The data were analyzed on the BioDeep Platform (https://www.biodeep.cn).

Statistical data analysis

SPSS 26.0 software (IBM Corporation, Armonk, USA) was used to analyze the data. Data are expressed as mean ± standard deviation(SD). In all cases, $P < 0.05$ was considered statistically significant. Prism 8 software (GraphPad, USA) is used to create graphs.

Results

H-2-104 significantly inhibited PSCs activity in vitro

The activity of PSCs after the intervention of H-2-104 is shown in Fig. 2A. The results showed that the activity of PSCs was inhibited to varying degrees after drug administration, with the inhibition in the group being significantly superior to that in the parent compound HM group. On the third day, the survival rate of PSCs in 200 µM H-2-104 group was 0%, which was significantly lower than that in HM group. The lethal concentration 50% (LC_{50}) of H-2-104 was 79.82 µM, significantly lower than that of HM at 109.1 µM (Fig. 2B). To investigate the effects of H-2-104 on the PSCs ultrastructure, SEM was used to observe the changes (Fig. 2C). After 48 h of intervention, the morphological structure of PSCs in DMSO group was intact, with a full body and neatly arranged microvilli. In HM group, the surface of PSCs was concave and the microvilli were messy; In the H-2-104 group, the surface of PSCs was wrinkled, the hook and microtriches were lost, and the body was seriously damaged.

Subchronic toxicity study to evaluate the safety of H-2-104

Throughout the treatment period, observations of fur coloration, behavioral patterns, dietary intake, and defecation status in all experimental groups revealed no abnormalities. Hematological parameters were quantitatively assessed, with corresponding results documented in Table 1. The WBC, Neu and Lym levels in HM group were significantly higher than those in control group ($P < 0.01$), while there was no significant difference in blood routine parameters between all H-2-104 groups and the control group ($P > 0.05$). Pathological results showed that chronic inflammatory cell infiltration occurred in the portal area of liver tissue and loose arrangement, swelling and deformation of brain tissue cells in HM group. However, no significant pathological changes were observed in the organs of mice in all dose groups of H-2-104 (Fig. 3A).

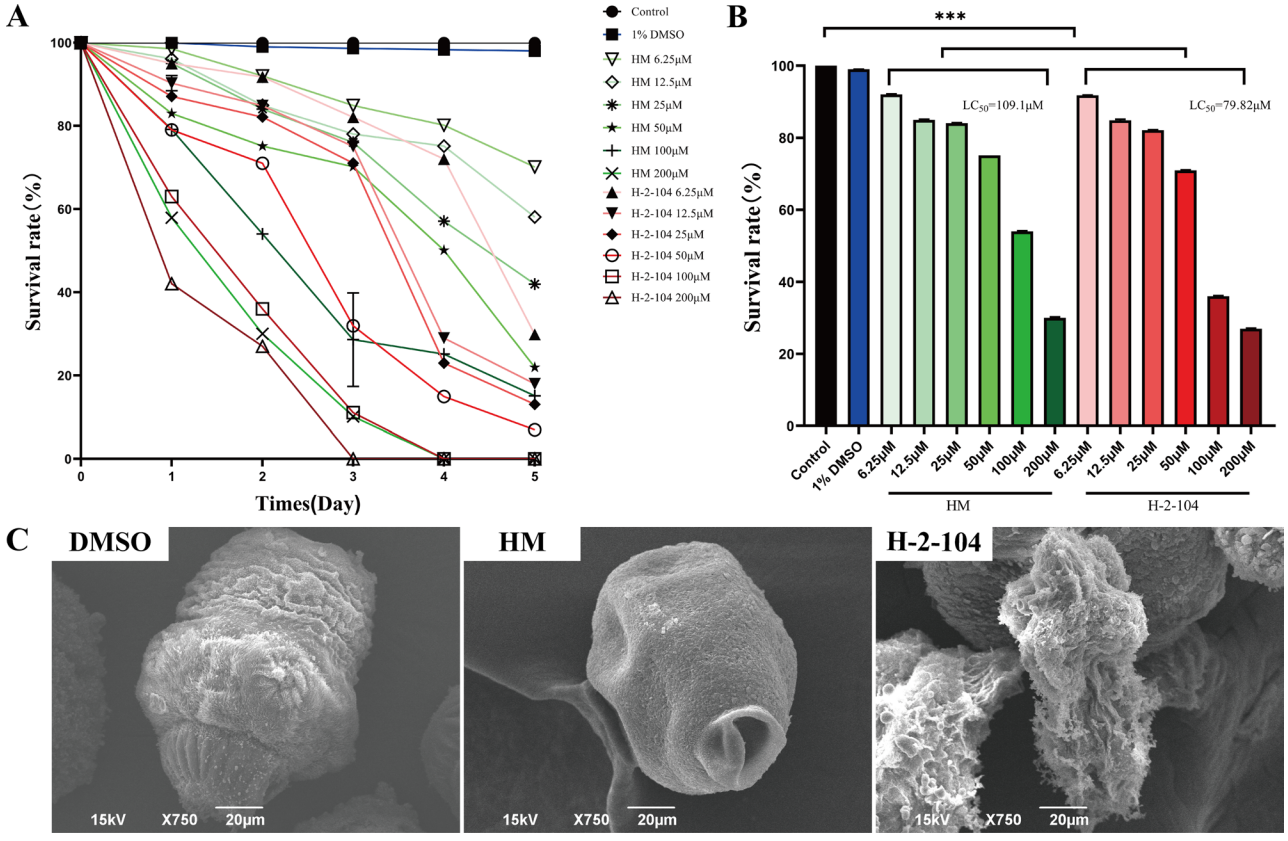

Fig. 2 The effects of H-2-104 on the activity and structure of PSCs. (**A**) PSCs activity(mean ± SD) after 5 days of intervention with gradient concentrations (**B**) PSCs activity(mean ± SD) after 48 h of intervention (**C**) Ultrastructure of PSCs observed under electron microscopy ($n = 3$) ***$P < 0.001$

Table 1 Effects of H-2-104 on the biochemical parameters of healthy KM mice after 30 days of intragastric administration (mean ± SD, $n = 6$)

Parameters	Control	HM	H-2-104		
	-	100 mg/kg	50 mg/kg	100 mg/kg	200 mg/kg
WBC(%)	8.70 ± 1.47	13.77 ± 2.12*	8.93 ± 0.94	8.61 ± 0.94	8.60 ± 0.87
Neu(%)	20.07 ± 1.36	27.33 ± 1.12*	20.88 ± 1.20	19.99 ± 1.65	19.86 ± 1.30
Lym(%)	71.06 ± 4.05	79.13 ± 3.94*	70.37 ± 4.18	69.82 ± 2.76	71.47 ± 2.77
Mon(%)	2.22 ± 0.27	2.02 ± 0.21	2.00 ± 0.19	2.21 ± 0.27	2.09 ± 0.26
Eos(%)	1.98 ± 0.22	2.04 ± 0.19	1.90 ± 0.19	1.99 ± 0.22	2.07 ± 0.21
RBC(10^{12}/L)	7.95 ± 0.41	7.85 ± 0.39	7.91 ± 0.41	7.86 ± 0.71	8.12 ± 0.31
HGB(g/L)	121.65 ± 9.88	126.53 ± 6.10	122.20 ± 4.60	120.87 ± 5.91	118.52 ± 6.53
AST(U/L)	118.21 ± 24.39	112.11 ± 20.71	115.25 ± 16.49	117.32 ± 19.35	114.63 ± 16.55
ALT(U/L)	42.12 ± 4.17	42.09 ± 4.04	43.14 ± 4.00	42.72 ± 4.38	44.44 ± 3.93
ALP(U/L)	29.09 ± 3.37	31.44 ± 3.54	27.46 ± 2.99	28.17 ± 3.20	28.54 ± 4.77
Cr(μM)	69.78 ± 4.44	67.35 ± 3.58	67.05 ± 3.81	67.74 ± 3.85	69.93 ± 3.83
BUN(mM)	8.30 ± 0.71	8.42 ± 0.56	8.21 ± 0.50	8.57 ± 0.46	8.75 ± 0.54

*Compared to the control group, $P < 0.01$

H-2-104 has therapeutic activity in vivo experiments in mice infected with *E. granulosus*

The in vivo efficacy of H-2-104 against *E. granulosus* cysts was investigated in KM mice infected with *E. granulosus*. Mice in the H-2-104 drug intervention group had significantly smaller cysts compared with mice in the model group and ABZ group (Fig. 3B). Therapeutic evaluation was performed through systematic analysis of cyst characteristics, including wet weight determination combined with morphological parameters (number and diameter of cysts), followed by inhibition rate computation to quantify treatment effects (Fig. 3C). Following 30-day treatment protocols, all therapeutic regimens demonstrated statistically significant improvements

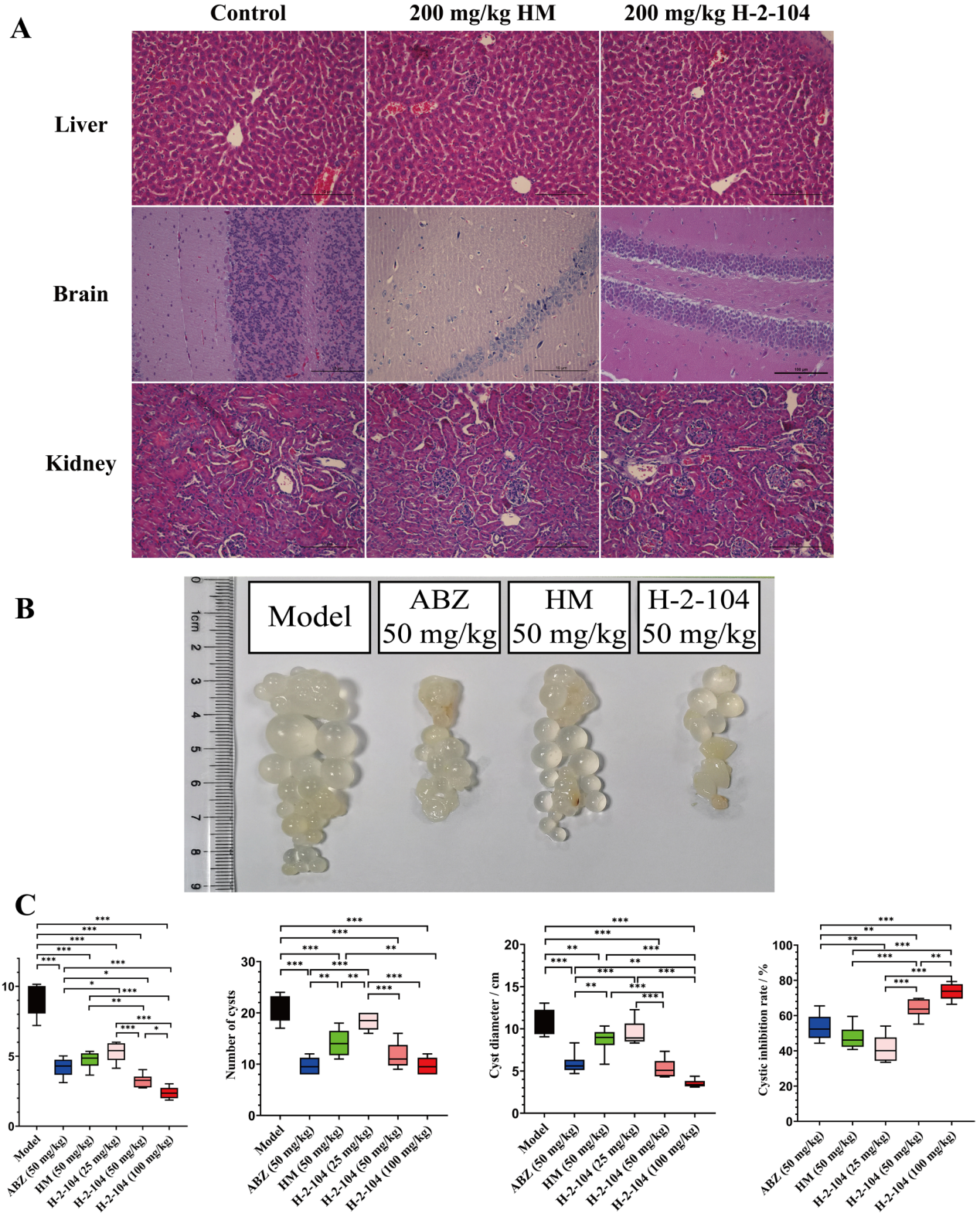

Fig. 3 (**A**) Effects of HM and H-2-104 on the tissue structure in healthy mice. Thirty days after treatment with HM and its derivatives, the mice were euthanized. HE staining was used to observe the histopathological changes in the livers, brains and kidneys of the mice. Bar = 10 μm. (**B**) Cyst size in mice after drug administration. (**C**) Cyst weight (mean ± SD), inhibition rate of capsule (mean ± SD), number of cysts(mean ± SD) and cyst diameter (mean ± SD) in mice ($n = 6$) *$P < 0.05$, **$P < 0.01$, ***$P < 0.001$

relative to the model group: cyst weight reduction (ANOVA, $F_{(5,\ 30)} = 63.601$, $P < 0.001$), decreased cyst count ($F_{(5,30)} = 27.031$, $P < 0.001$), reduced cyst diameter ($F_{(5,\ 30)} = 27.532$, $P < 0.001$), and elevated inhibition rates ($F_{(5,\ 30)} = 112.820$, $P < 0.001$). H-2-104 displayed dose-responsive therapeutic profiles across its dosage range (25, 50 and 100 mg/kg). Particularly noteworthy was the 50 mg/kg dose, which achieved equivalent or enhanced efficacy compared to both ABZ and HM at iso-dosage levels (50 mg/kg), whereas maximal therapeutic response was attained with the 100 mg/kg regimen.

H-2-104 attenuated liver damage in mice infected with *E. granulosus*

The HE staining results revealed that the liver tissue of mice in the model group exhibited obvious pathological changes, with vesicular structures visible in the center and hepatocytes arranged in disarray. In the ABZ group, cysts were also observed in liver tissue, but they were characterized by clear structure and distinct boundaries, suggesting absorption of vesicular contents. No significant pathological changes were noted in the liver tissues of mice in the various H-2-104 groups(Fig. 4A). The Masson staining results indicated that there was significant collagen deposition in the model group, while the ABZ group showed marked improvement in this regard. All H-2-104 groups demonstrated significant improvement in collagen deposition, with the level of improvement increasing significantly as the drug dosage increased (ANOVA, $F_{(5,30)} = 231.339$, $P < 0.05$). Specifically, the improvement observed in the 50 mg/kg H-2-104 group was comparable to that in the ABZ group, with no statistical difference. However, the effect of the 100 mg/kg H-2-104 group was significantly superior to that of the ABZ group(Fig. 4B).

H-2-104 destroys the normal structure of cysts infected with *E. granulosus* in mice in vivo

The results of TEM on *E. granulosus* cysts revealed the following (Fig. 5): In the model group, the vesicular wall structure of *E. granulosus* was clear and intact, with distinct boundaries between the cortical and germinal layers. The nuclei, nuclear membranes, and nucleoli were clearly visible, and the microvilli on the vesicular wall were arranged neatly and uniformly in length. In the ABZ group, the vesicular wall thickness of *E. granulosus* was significantly uneven, with a disorganized germinal layer that was difficult to distinguish. Nuclear rupture was observed, and the microvilli varied in length, with a significant increase in vacuolar structures. In the 25 mg/kg H-2-104 group, the cyst wall of *E. granulosus* was thickened, with a clear separation between the germinal and cortical layers, and sparse microvilli. In the 50 mg/kg H-2-104 group, the cyst wall structure of *E. granulosus* was unclear, with the cortical and germinal layers intertwined. Pyknosis

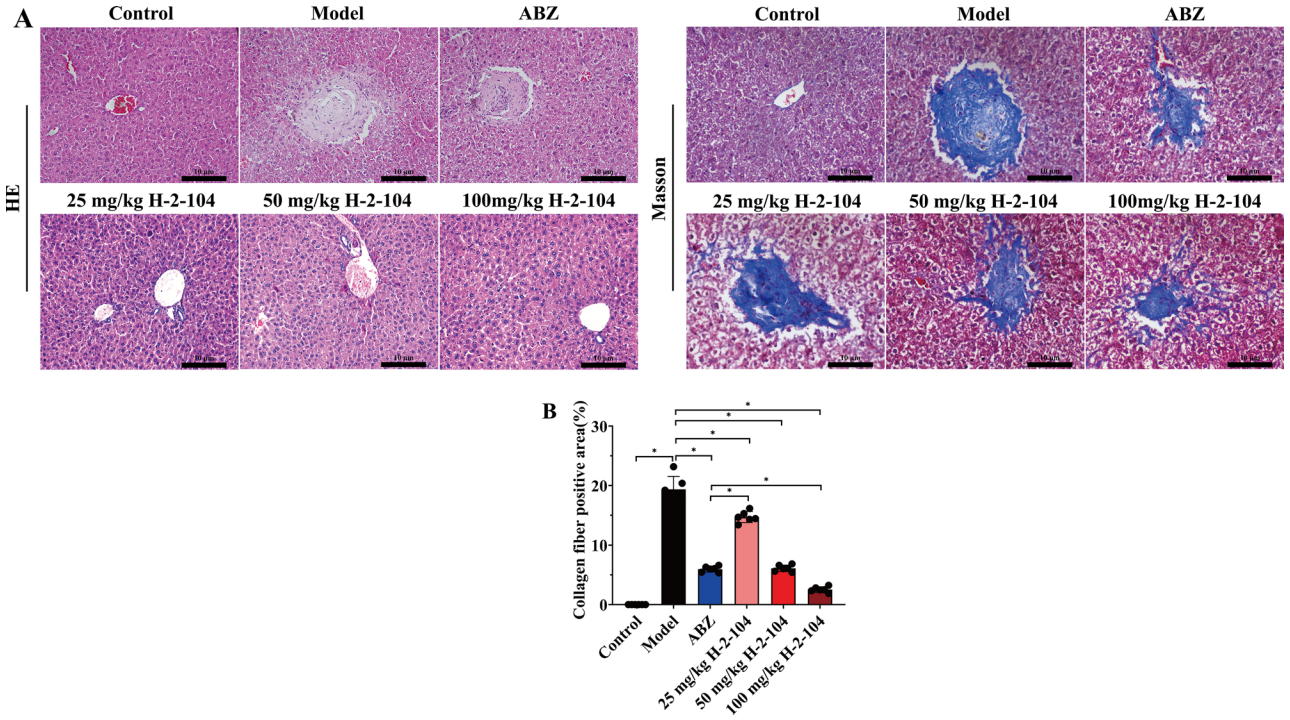

Fig. 4 Pathologic changes in the liver in each group. (**A**) HE staining and masson staining results. (**B**) Quantitative analysis of masson staining. Scale bar = 10 μm ($n = 6$) *$P < 0.05$

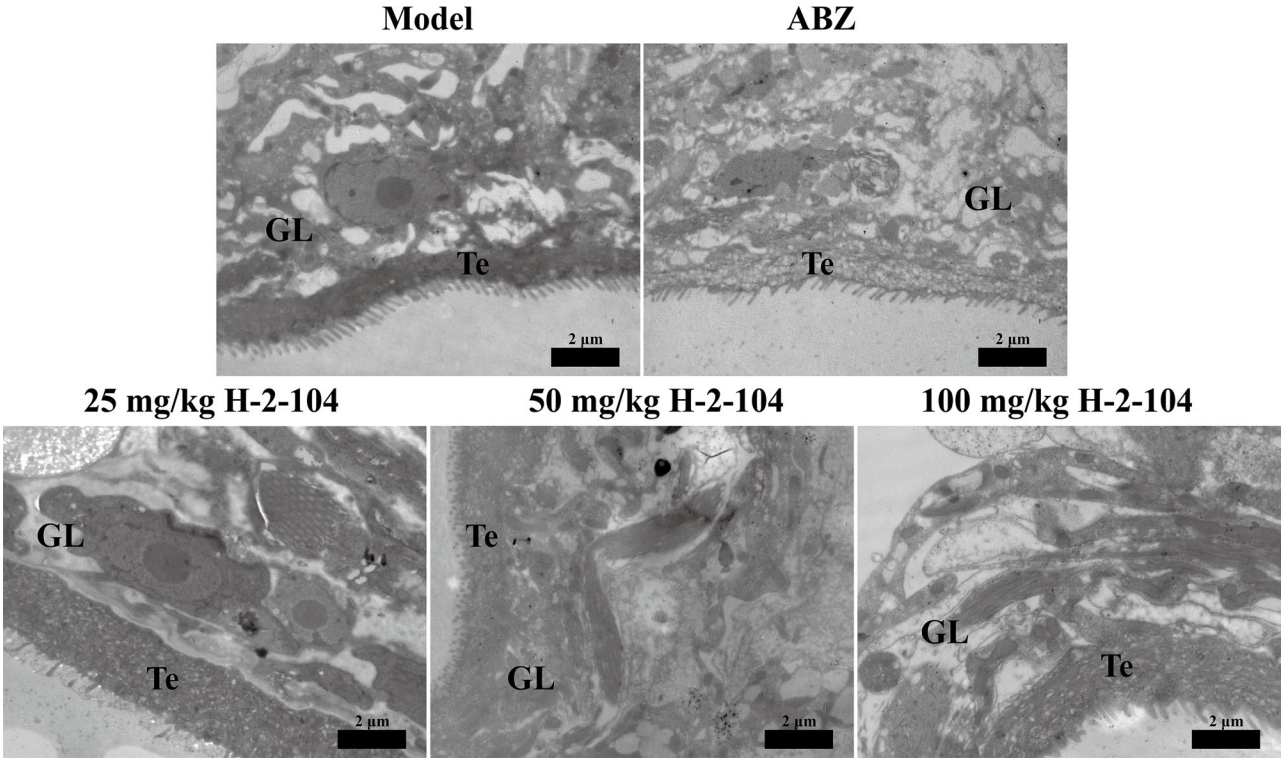

Fig. 5 Cyst ultrastructural changes. GL: Germinal layers; Te: tegument. Scale bar = 2 μm

and fragmented tissues were visible in the germinal layer, and the microvilli were disorganized. In the 100 mg/kg H-2-104 group, the cyst wall of *E. granulosus* was significantly thickened, with the structures of the germinal layer appearing layered and an increase in elongated vacuolar structures. The microvilli varied in length and thickness. These findings suggest that both the ABZ group and the various H-2-104 groups have certain destructive and damaging effects on the cysts of *E. granulosus*.

Serum metabolomics analysis

In the PCA analysis, the R^2X values were 0.514 and 0.539, respectively (Fig. 6A, B), indicating certain distinctions among the sample groups, though further screening of inter-group differences is required. To proceed, OPLS-DA was employed for data analysis (Fig. 6C, D,E, F). Additionally, to validate the model's effectiveness, 200 permutation tests were conducted (Fig. 6G, H,I, J). The results demonstrated that, in positive ion mode, the R^2X, R^2Y, and Q^2 for the control and model groups were 0.467, 0.999, and 0.834, respectively, while in negative ion mode, these values were 0.396, 0.990, and 0.825 for the same groups. For the model and H-2-104 groups, in positive ion mode, the R^2X, R^2Y, and Q^2 were 0.354, 0.981, and 0.726, respectively, and in negative ion mode, the corresponding values were 0.484, 0.996, and 0.752. These results indicate that there are significant differences between control group and model group, model group and H-2-104 group, and Q^2 of each model is greater than 0.5, which indicates that the model has a good prediction degree. Furthermore, with Q^2 values greater than 0.5 for all models, the predictive performance of the models is considered good.

Based on the OPLS-DA model, differential metabolites between the control group and model group, as well as between the model group and H-2-104 group, were screened using the criteria of Variable Importance in the Projection (VIP) > 1 and $P < 0.05$. Compared with the control group, a total of 1401 differential metabolites were significantly altered ($P < 0.05$) in the model group, with 611 upregulated and 790 downregulated (Fig. 6K). These metabolites can serve as potential biomarkers to characterize metabolic disturbances in the body following *E. granulosus* infection. Compared with the model group, a total of 914 differential metabolites were significantly altered ($P < 0.05$) in the H-2-104 group, with 399 upregulated and 515 downregulated (Fig. 6L). By comparing the differential metabolites obtained from the two inter-group screenings and utilizing the KEGG database to compare the significantly different metabolites, it was found that 64 differential metabolites were significantly altered ($P < 0.05$) in both inter-group comparisons (Table S1). To visually compare the content

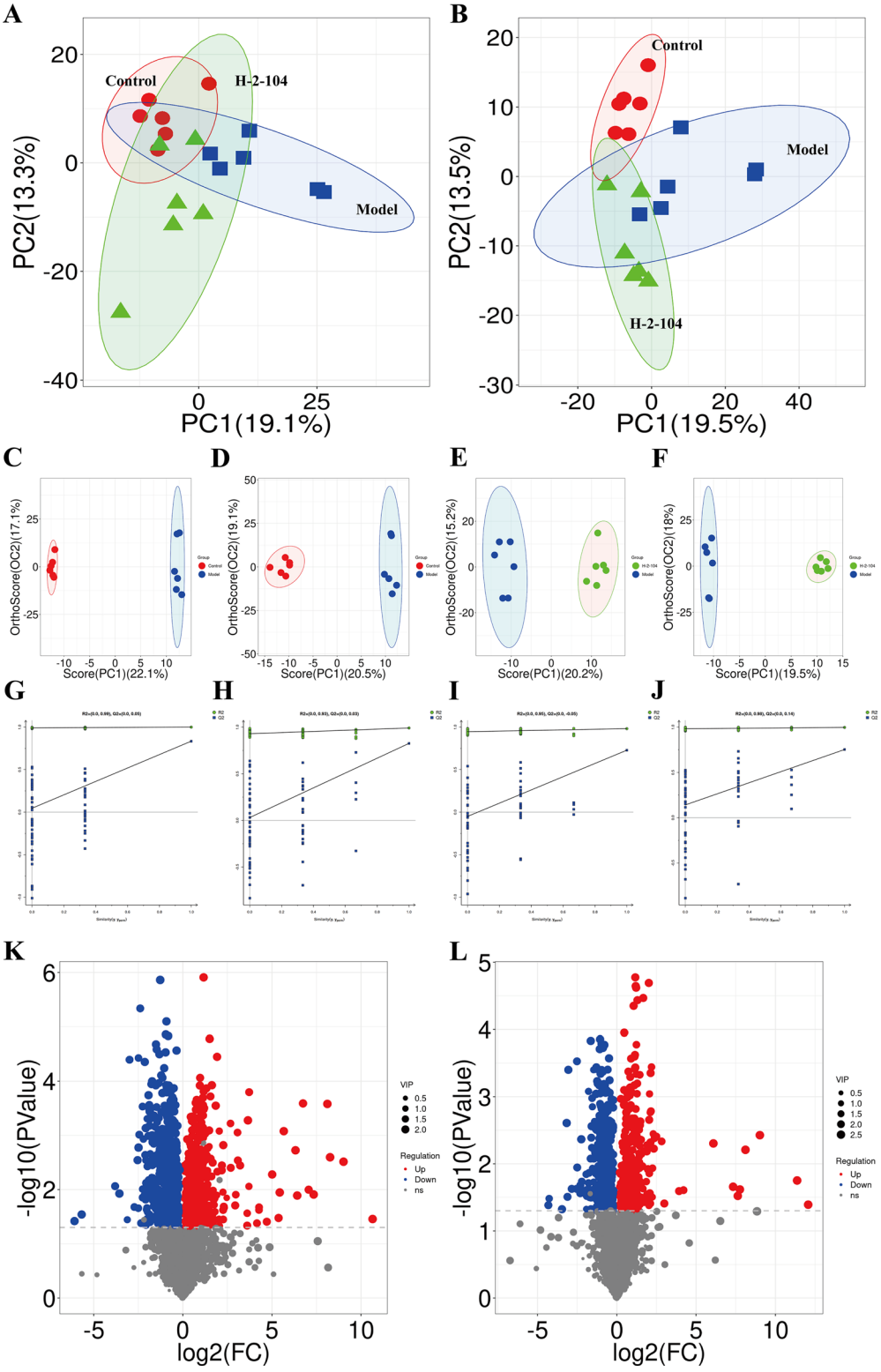

Fig. 6 Multivariate statistical analysis of serum samples. (**A**, **B**) PCA score plots, (**C**, **E**) OPLS-DA score plots in positive ion mode, (**D**, **F**) OPLS-DA score plots in negative ion mode, (**G**, **I**) OPLS-DA permutation plots in positive ion mode, (**H**, **J**) OPLS-DA permutation plots in negative ion mode, (**K**) Volcano plot in control group vs. model group and (**L**) Volcano plot in model group vs. H-2-104 group

changes of the common differential metabolites among the groups, the content of these 64 differential metabolites in each sample was converted into a clustered heatmap (Fig. 7A).

Pathway enrichment analysis was conducted on the 64 differential metabolites using the KEGG database (Fig. 7B). The main pathways with significant differences in the serum before and after drug administration include Necroptosis, Choline metabolism in cancer, Retrograde endocannabinoid signaling, Linoleic acid metabolism, Phenylalanine metabolism, and others.

Liver metabolomics analysis

In the PCA analysis, the R^2X values were 0.562 and 0.541, respectively (Fig. 8A, B), indicating the presence of certain differences among the sample groups, but further screening for inter-group differences was necessary. To further analyze the data, OPLS-DA was employed (Fig. 8C, D,E, F). Additionally, to validate the effectiveness of the models, 200 permutation tests were conducted for each (Fig. 8G, H,I, J). The results showed that for the control and model groups in positive ion mode, the R^2X, R^2Y, and Q^2 values were 0.47, 0.994, and 0.856, respectively. In negative ion mode, the corresponding values for these two groups were 0.503, 0.996, and 0.816. For the model and H-2-104 groups in positive ion mode, the R^2X, R^2Y, and Q^2 values were 0.281, 0.991, and 0.664, respectively, while in negative ion mode, the values were 0.302, 0.98, and 0.584. These results indicate that there are significant differences between the control and model groups, as well as between the model and H-2-104 groups. Furthermore, the Q^2 values of all models were greater than 0.5, indicating good predictive performance of the models.

Based on the OPLS-DA model, differential metabolites between the control and model groups, as well as between the model and H-2-104 groups, were screened using the criteria of Variable Importance in the Projection (VIP) > 1 and $P < 0.05$, and volcano plots were generated for each comparison. Compared to the control group, a total of 2,039 differential metabolites were significantly altered ($P < 0.05$) in the model group, with 1,209 upregulated and 830 downregulated (Fig. 8K). These metabolites can serve as potential biomarkers indicating metabolic disturbances in the body following *E. granulosus* infection. In comparison to the model group, 900 differential metabolites were significantly changed ($P < 0.05$) in the H-2-104 group, including 417 upregulated and 483 downregulated (Fig. 8L).

By comparing the differential metabolites obtained from the two inter-group screenings and utilizing the KEGG database for further analysis of significantly different metabolites, it was found that 81 differential metabolites were significantly altered ($P < 0.05$) in both comparisons (Table S2). To visually compare the changes in the abundance of these common differential metabolites across the groups, the abundances of these 81 differential metabolites in each sample were converted into a clustered heatmap (Fig. 9A).

Pathway enrichment analysis was conducted for 81 differential metabolites based on the KEGG database, and the results were visually presented (Fig. 9B). The major pathways with significant differences in the serum before and after drug administration primarily included Fructose and mannose metabolism, Phosphotransferase system (PTS), and Retrograde endocannabinoid signaling.

Discussion

Numerous studies have reported that HM has a good inhibitory effect on *E. granulosus*, but its obvious neurotoxicity limits the clinical application of HM. Therefore, in order to reduce the toxicity and increase the efficacy, our team synthesized 1,076 new compounds including 32 types of structures by structural modification of 1, 2, 3, 7, and 9 positions of HM parent nucleus. The pharmacodynamics and subchronic toxicity results in vitro and in vivo showed that H-2-104 might be a promising compound for the treatment of echinococcosis caused by *E. granulosus* infection, and the mechanism might be related to the regulation of necroptosis, linoleic acid metabolism, phenylalanine metabolism, glucose metabolism and lipid metabolism.

Our previous study showed that derivatives DH-330, H-2-98 and H-2-168 possessed potent anti-CE activities [62]. In this study, the anti-hydatid effect of derivative H-2-104 was investigated on the basis of previous studies.The results in vitro showed that all the *E. granulosus* treated with 200 μm of H-2-104 died on the third day of intervention, which was much better than that of HM at the same concentration. Currently, although drugs for CE have been widely developed and have shown significant parasiticidal effects in vitro, but the in vivo effects are unsatisfactory. Therefore, we further evaluated the therapeutic efficacy of H-2-104 in *E. granulosus* infected mice. The of subchronic results showed that thesafety of H-2-104 was significantly better than that of HM, and was equivalent to that of ABZ. At the same dosage of 50 mg/kg/day, the treatment effect of H-2-104 was significantly better than that of ABZ. The TEM results further demonstrated that after treatment with H-2-104, the ultrastructure of the cysts was disrupted to different degrees. These results suggest that H-2-104 may be a promising new drug against echinococcosis.

In order to clarify the anti-echinococcosis mechanism of H-2-104, the changes of metabolites in serum and liver of mice before and after H-2-104 intervention

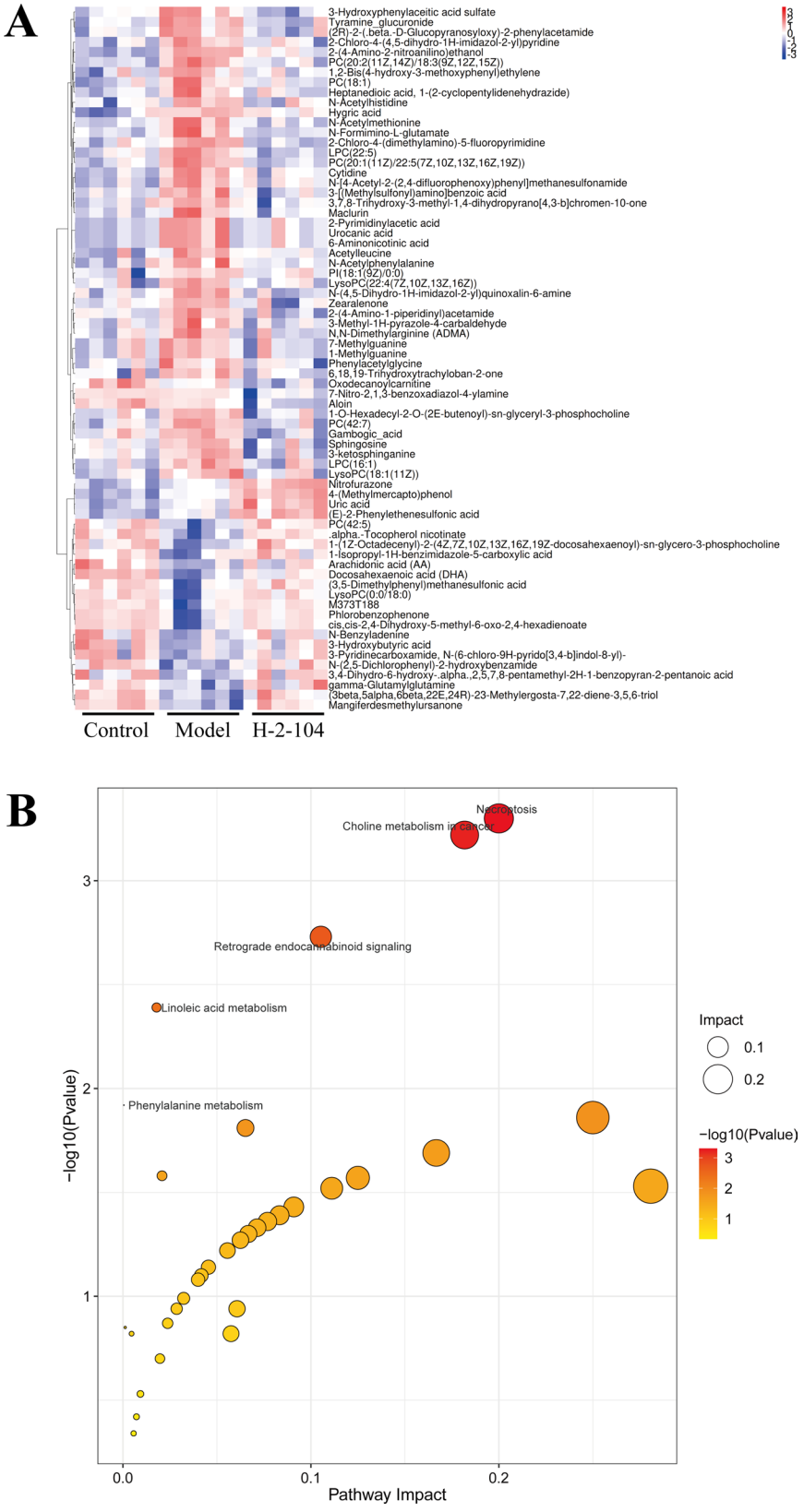

Fig. 7 Differential metabolite classification and metabolite pathway enrichment analysis of serum samples. (**A**) Differential metabolite classification. (**B**) Metabolite pathway enrichment analysis

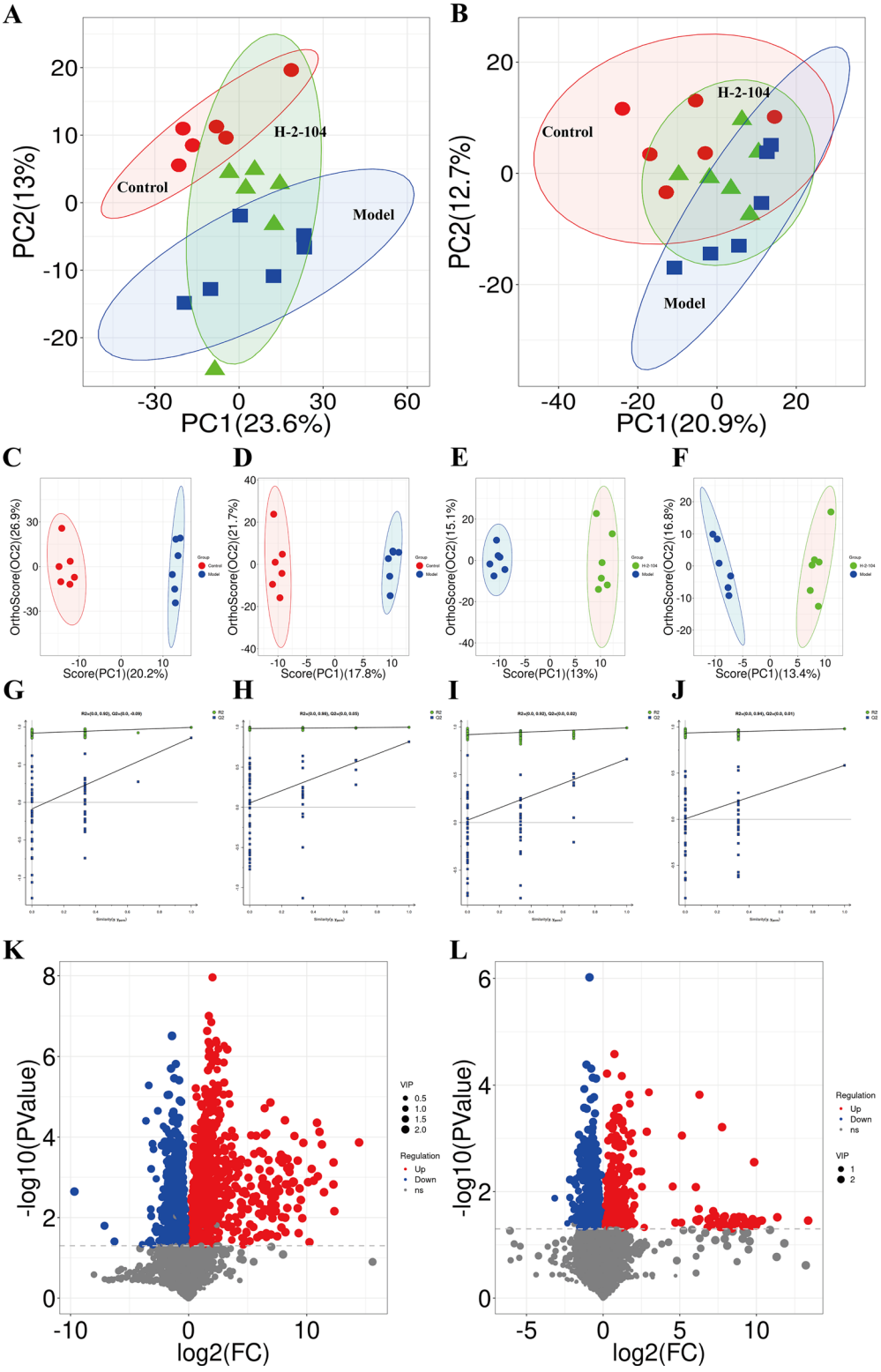

Fig. 8 Multivariate statistical analysis of liver samples. (**A**, **B**) PCA score plots, (**C**, **E**) OPLS-DA score plots in positive ion mode, (**D**, **F**) OPLS-DA score plots in negative ion mode, (**G**, **I**) OPLS-DA permutation plots in positive ion mode, (**H**, **J**) OPLS-DA permutation plots in negative ion mode, (**K**) Volcano plot in control group vs. model group and (**L**) Volcano plot in model group vs. H-2-104 group

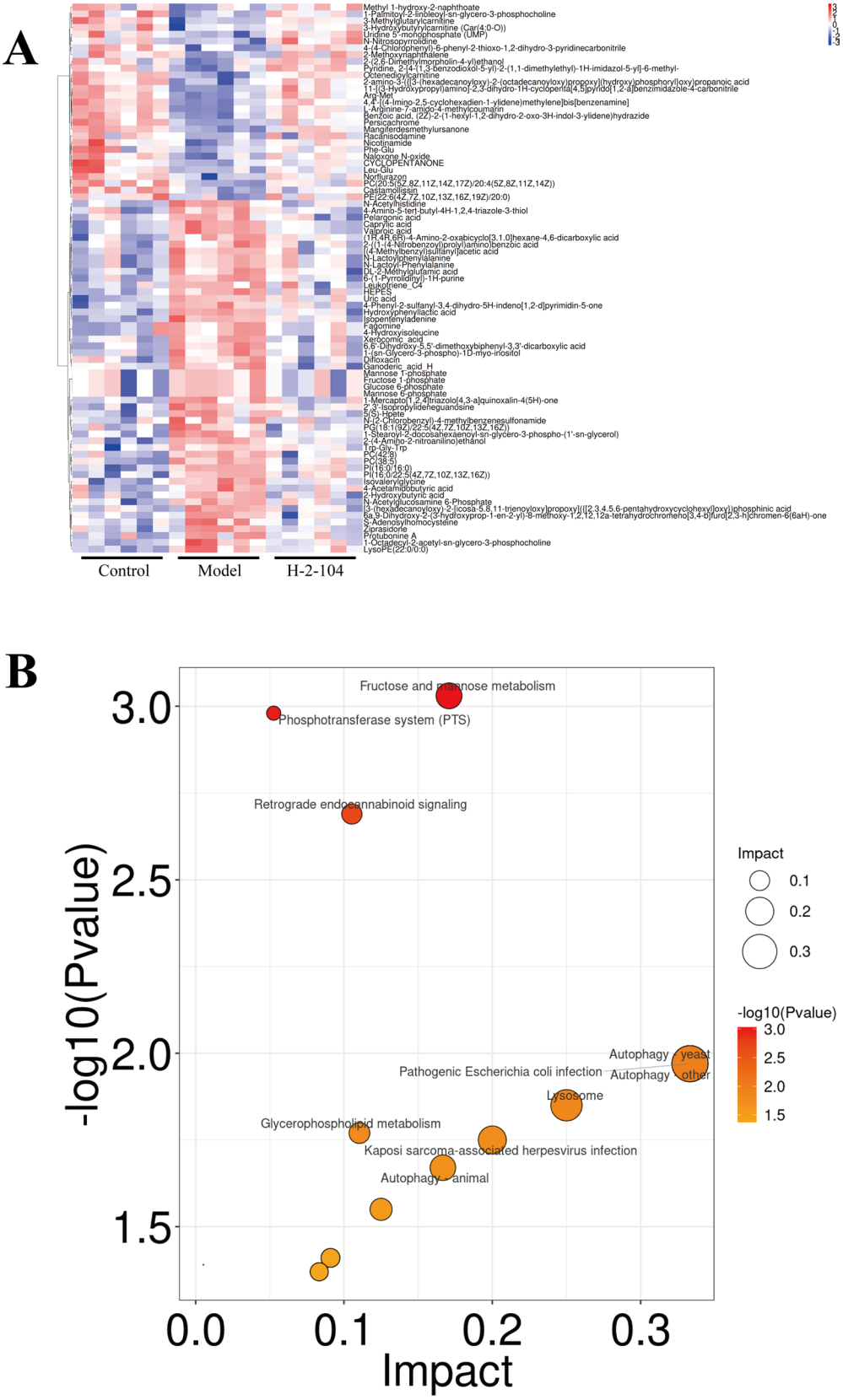

Fig. 9 Differential metabolite classification and metabolite pathway enrichment analysis of liver samples. (**A**) Differential metabolite classification. (**B**) metabolite pathway enrichment analysis

were further investigated by non-targeted metabolomics. In serum metabolomics studies, the concentrations of a total of 64 metabolites underwent significant changes after model establishment and were altered following H-2-104 intervention. The enriched metabolic pathways primarily included necroptosis, linoleic acid metabolism, and phenylalanine metabolism. Necroptosis [63], a form of programmed cell death, is activated by extracellular or intracellular signals when apoptosis is blocked and occurs widely in various liver diseases such as hepatitis and liver cancer. Studies have shown that necroptosis can promote liver pathology, hepatocyte injury, and death [64–66]. When necroptosis occurs in multiple types of liver cells, including hepatic stellate cells and Kupffer, inflammatory mediators are released, leading to inflammatory lesions and fibrosis in the liver. Inducing the death of these cells or inhibiting their functions can slow down or even reverse the progression of liver fibrosis [67, 68]. Recent studies have confirmed that harmine has a certain ameliorative effect on acute liver injury induced by CCl_4, with mechanisms related to necroptosis [69]. In the present study, Masson staining results showed that H-2-104 could significantly improve the area of collagen deposition in the liver, suggesting that H-2-104 may have the effect of alleviating liver fibrosis caused by *E. granulosus*, and its mechanism may be related to necroptosis. Arachidonic acid (AA) and its metabolites, as well as sphingosine, can activate or inhibit certain signaling pathways, further regulating cell survival or death [70]. In this study, the differential metabolites arachidonic acid and sphingosine jointly participated in the necroptosis pathway, suggesting that H-2-104 may improve liver damage caused by *E. granulosus* by altering metabolite concentrations and regulating the necroptosis pathway.

Linoleic acid, as an unsaturated fatty acid, possesses antioxidant properties that can neutralize free radicals in the body and reduce oxidative stress-induced damage to hepatocytes [71]. It also participates in linoleic acid metabolism within organisms. Multiple research findings have indicated a link between the linoleic acid metabolic pathway and liver function, suggesting that drugs can improve normal liver physiological functions by regulating this pathway [72, 73]. The improvement of *E. granulosus* by H-2-104 may be related to this pathway. Additionally, differential metabolites such as N-acetylphenylalanine and phenylacetylglycine participate in the phenylalanine metabolic pathway, which primarily occurs in liver tissue and involves the conversion of phenylalanine to tyrosine under enzymatic catalysis [74]. The normal functioning of the liver directly affects the phenylalanine metabolic pathway, particularly during inflammation or infection, which can lead to increased phenylalanine levels in the body [75], consistent with the results of this study. Some studies have also found that abnormalities in certain enzymes within the phenylalanine metabolic pathway can produce metabolites that activate specific signaling pathways, thereby exacerbating liver diseases. Furthermore, research has shown that the phenylalanine metabolic pathway is disturbed in the livers of mice infected with *E. granulosus* [76]. Combined with the regulation of the phenylalanine metabolic pathway observed in this study following drug intervention, it can be inferred that the efficacy of H-2-104 may be related to its regulation of phenylalanine metabolism and key substances within this pathway. Future exploration of this pathway and its key substances as potential drug targets holds significant research value.

In liver metabolomics research, the concentrations of a total of 81 metabolites underwent significant changes after model establishment and were altered following H-2-104 intervention. The enriched metabolic pathways primarily included fructose and mannose metabolism, glycerophospholipid metabolism, and others. In this study, 6-phosphoglucomannose, 1-phosphoglucomannose, and fructose-6-phosphate collectively participated in the fructose and mannose metabolic pathway [77], further influencing glucose metabolism in the organism. 6-Phosphoglucomannose is an intermediate in the metabolic pathway, with its primary metabolism involving conversion to fructose-6-phosphate by an isomerase for glycolysis, and its secondary metabolism involving conversion to 1-phosphoglucomannose by a mutase for protein glycosylation [78]. *E. granulosus* primarily maintains its life activities through glycolysis for energy production. For the growth and development of parasites, acquiring energy sources from the host is extremely important [79]. Glucose is the primary energy substance for *E. granulosus* to maintain life activities, and blocking the parasite's energy acquisition is an effective means to inhibit its growth. The metabolomics results also suggest that H-2-104 may interfere with the organism's glucose metabolism process to exert an inhibitory effect on *E. granulosus*. Additionally, enrichment results revealed changes in glycerophospholipid metabolism within the organism. Glycerophospholipid metabolism is part of lipid metabolism, and lipids play crucial roles in transmitting intercellular signals, maintaining cell survival and apoptosis, and sustaining normal organismal functions [80, 81]. Diseases or drugs can disrupt this metabolic pathway, further causing liver damage [28]. Based on the experimental results, it is speculated that H-2-104 may also normalize the disordered glycerophospholipid metabolism in the organism, thereby restoring proper function and overcoming the damage caused by *E. granulosus* to the liver.

The limitations of this study are as follows. First, although the sub-chronic toxicity results indicated that H-2-104 was safe, its long-term toxicity remains unclear

and requires further observation. Secondly, additional samples are necessary to validate the current results and enhance the reliability and accuracy of the procedure. Finally, various omics technologies, such as transcriptomics and proteomics, could be cross-validated to better support the experimental findings. In summary, this study systematically investigated the anti-echinococcosis effect of H-2-104 both in vitro and in vivo, and explored the potential mechanism of H-2-104 in treating *E. granulosus* infection in mice using non-targeted metabolomics. This research offers a novel strategy for anti-CE drug treatment.

Conclusions

In conclusion, this study systematically investigated the anti-echinococcosis effects of the harmine derivative H-2-104, both in vitro and in vivo. The results demonstrated that H-2-104 exhibited significant inhibitory activity against *E. granulosus*, suggesting that H-2-104 may represent a promising new drug for the treatment of CE. Furthermore, its anti-CE effects may be associated with the regulation of multiple pathways, including apoptosis, amino acid metabolism, and glucose metabolism. Future studies should further explore H-2-104 and its related pathways as key areas of interest.

Abbreviations

CE	Cystic echinococcosis
E. granulosus	*Echinococcus granulosus*
PSCs	Protoscoleces
WHO	World Health Organization
FAO	Food and Agriculture Organization
WBC	White blood cell
Neu	Neutrophil
Lym	Lymphocyte
Mon	Monocyte
Eos	Eosinophil
RBC	Red blood cell
HGB	Hemoglobin
AST	Aspartate aminotransferase
ALT	Alanine aminotransferase
ALP	Alkaline phosphatase
Cr	Creatinine
BUN	Blood urea nitrogen
SEM	Scanning electron microscope
TEM	Transmission Electron Microscope
DMSO	Dimethyl sulfoxide
HE	Hematoxylin-eosin staining
PCA	Principal Component Analysis
PLS-DA	Partial Least Squares Discriminant Analysis
OPLS-DA	Orthogonal Partial Least Squares Discriminant Analysis
KEGG	Kyoto Encyclopedia of Genes and Genomes

Supplementary Information

The online version contains supplementary material available at https://doi.org/10.1186/s12917-025-04642-x.

Supplementary Material 1

Supplementary Material 2

Acknowledgements

Not applicable.

Author contributions

LT and HJG designed the study, and critically revised the manuscript. HJG, QWX and KK performed the experiment. QWX, Jiang Z and KA analyzed the metabolomic data. BC and Jun Z drafted the manuscript. All authors read and approved the final manuscript.

Funding

This work was supported by Xinjiang Uygur Autonomous Region Key Research and Development Project (No.2022B03013-4), Open Subject of State Key Laboratory of Pathogenesis, Prevention and Treatment of High Incidence Diseases in Central Asia (SKL-HIDCA-2022-BC3, SKL-HIDCA-2023-YX1), Xinjiang Uygur Autonomous Region Natural Science Foundation (2023D01D16, 2023D01A120), China International Medical Exchange Foundation-Clinical Pharmacy Branch of Chinese Medical Association 2023 Clinical Pharmacy Research Fund (Z-2021-46-2101-2023), Xinjiang Production and Construction Corps Science and Technology Tackling Program Projects (2023AB009-04).

Data availability

Data supporting the conclusions of this article are included within the article.

Declarations

Ethics approval and consent to participate

The animal procedures were approved by the Animal Ethical Committee of Xinjiang Medical University with the approval number IACUC-20170420-04.

Consent to participate

Not applicable.

Consent for publication

Not applicable.

Competing interests

The authors declare no competing interests.

Author details

[1]Department of Pharmacy, The First Affiliated Hospital of Xinjiang Medical University, Urumqi 830054, China
[2]State Key Laboratory of Pathogenesis, Prevention and Treatment of High Incidence Diseases in Central Asia, Xinjiang Medical University, Urumqi 830000, China
[3]College of Pharmacy, Xinjiang Medical University, Urumqi 830000, China
[4]Department of Abdominal Surgery, The Third People Hospital of Xinjiang Uygur Autonomous Region, Urumqi 831399, China
[5]School of Environmental and Biological Engineering, Nanjing University of Science and Technology, Nanjing 210094, China
[6]Clinical Medicine Institute, The First Affiliated Hospital of Xinjiang Medical University, Urumqi 830054, China

Received: 11 February 2025 / Accepted: 4 March 2025
Published online: 17 March 2025

References

1. Yin J, Liu C, Shen Y, Zhang H, Cao J. Efficacy of ursolic acid against Echinococcus granulosus in vitro and in a murine infection model. Parasit Vectors. 2018;11:58.
2. Larrieu E, Gavidia CM, Lightowlers MW. Control of cystic echinococcosis: background and prospects. Zoonoses Public Health. 2019;66:889–99.
3. Agudelo Higuita NI, Brunetti E, McCloskey C. Cystic echinococcosis. J Clin Microbiol. 2016;54:518–23.
4. Joanny G, Mehmood N, Dessì G, Tamponi C, Nonnis F, Hosri C, Saarma U, Varcasia A, Scala A. Cystic echinococcosis in sheep and goats of Lebanon. Parasitology. 2021;148:871–8.
5. Khan A, Ahmed H, Khan H, Saleem S, Simsek S, Brunetti E, Afzal MS, Manciulli T, Budke CM. Cystic echinococcosis in Pakistan: A review of reported cases, diagnosis, and management. Acta Trop. 2020;212:105709.

6. Alvi MA, Ali RMA, Khan S, Saqib M, Qamar W, Li L, Fu BQ, Yan HB, Jia WZ. Past and present of diagnosis of echinococcosis: A review (1999–2021). Acta Trop. 2023;243:106925.
7. Ma T, Wang Q, Hao M, Xue C, Wang X, Han S, Wang Q, Zhao J, Ma X, Wu X, Jiang X, Cao L, Yang Y, Feng Y, Gongsang Q, Scheffran J, Fang L, Maude RJ, Zheng C, Ding F, Wu W, Jiang D. Epidemiological characteristics and risk factors for cystic and alveolar echinococcosis in China: an analysis of a National population-based field survey. Parasit Vectors. 2023;16:181.
8. Huang D, Li R, Qiu J, Sun X, Yuan R, Shi Y, Qu Y, Niu Y. Geographical environment factors and risk mapping of human cystic echinococcosis in Western China. Int J Environ Res Public Health. 2018;15:1729.
9. Wen H, Vuitton L, Tuxun T, Li J, Vuitton DA, Zhang W, McManus DP. Echinococcosis: advances in the 21st century. Clin Microbiol Rev. 2019;32:e00075–18.
10. Gu H, Hu Y, Guo S, Jin Y, Chen W, Huang C, Hu Z, Li F, Liu J. China's prevention and control experience of echinococcosis: A 19-year retrospective. J Helminthol. 2024;98:e16.
11. Zhou T, Xu X, Zhu J, Aizezi M, Aierken A, Meng M, He R, Aimulajiang K, Wen H. Association of IL-9 cytokines with hepatic injury in Echinococcus granulosus infection. Biomolecules. 2024;14:1007.
12. Jiang N, Chen Y, Li T, Sun Y, Su Y, Wang Y, Shen Y, Cao J. Proteomic analysis of mouse liver lesions at all three stages of Echinococcus granulosus infection. PLoS Negl Trop Dis. 2024;18:e0012659.
13. Wen L, Lv G, Zhao J, Lu S, Gong Y, Li Y, Zheng H, Chen B, Gao H, Tian C, Wang J. In vitro and in vivo effects of artesunate on *Echinococcus granulosus* protoscoleces and metacestodes. Drug Des Devel Ther. 2020;14:4685–94.
14. Brunetti E, Kern P, Vuitton DA. Expert consensus for the diagnosis and treatment of cystic and alveolar echinococcosis in humans. Acta Trop. 2010;114:1–16.
15. Solomon N, Kachani M, Zeyhle E, Macpherson CNL. The natural history of cystic echinococcosis in untreated and albendazole-treated patients. Acta Trop. 2017;171:52–7.
16. Pensel P, Paredes A, Albani CM, Allemandi D, Sanchez Bruni S, Palma SD, Elissondo MC. Albendazole nanocrystals in experimental alveolar echinococcosis: enhanced chemoprophylactic and clinical efficacy in infected mice. Vet Parasitol. 2018;251:78–84.
17. Pensel PE, Castro S, Allemandi D, Bruni SS, Palma SD, Elissondo MC. Enhanced chemoprophylactic and clinical efficacy of albendazole formulated as solid dispersions in experimental cystic echinococcosis. Vet Parasitol. 2014;203:80–6.
18. Wang W, Li J, Yao J, Wang T, Li S, Zheng X, Duan L, Zhang W. In vitro and in vivo efficacies of novel carbazole aminoalcohols in the treatment of cystic echinococcosis. J Antimicrob Chemother. 2017;72:3122–30.
19. Grüner B, Kern P, Mayer B, Gräter T, Hillenbrand A, Barth TEF, Muche R, Henne-Bruns D, Kratzer W, Kern P. Comprehensive diagnosis and treatment of alveolar echinococcosis: A single-center, long-term observational study of 312 patients in Germany. GMS Infect Dis. 2017;5:Doc01.
20. Al-Abodi HR, Al-Shadeedi SMJ, Ghasemian KZKA. Zataria multiflora bois as an auspicious therapeutic approach against Echinococcus granulosus: current status and future perspectives. Comp Immunol Microbiol Infect Dis. 2019;66:101335.
21. Karimi Yazdi M, Haniloo A, Ghaffari A, Torabi N. Antiparasitic effects of Zataria multiflora essential oil nano-emulsion on larval stages of Echinococcus granulosus. J Parasit Dis. 2020;44:429–35.
22. Mahmoudvand H, Dezaki ES, Kheirandish F, Ezatpour B, Jahanbakhsh S, Harandi MF. Scolicidal effects of black Cumin seed (Nigella sativa) essential oil on hydatid cysts. Korean J Parasitol. 2014;52:653–9.
23. Rouhani S, Salehi N, Kamalinejad M, Zayeri F. Efficacy of Berberis vulgaris aqueous extract on viability of Echinococcus granulosus protoscolices. J Invest Surg. 2013;26:347–51.
24. Haji Mohammadi KH, Heidarpour M, Borji H. In vivo therapeutic efficacy of the Allium sativum ME in experimentally Echinococcus granulosus infected mice. Comp Immunol Microbiol Infect Dis. 2018;60:23–7.
25. Moazeni M, Nazer A. In vitro effectiveness of Garlic (Allium sativum) extract on scolices of hydatid cyst. World J Surg. 2010;34:2677–81.
26. Liu C, Fan H, Guan L, Ge RL, Ma L. In vivo and in vitro efficacy of Crocin against Echinococcus multilocularis. Parasit Vectors. 2021;14:364.
27. Aghighi K, Heidarpour M, Borji H. The anti-echinococcal activity of Crocin in mice experimentally infected with Echinococcus granulosus. Exp Parasitol. 2023;246:108463.
28. Mina CN, Farzaei MH, Gholamreza A. Medicinal properties of Peganum harmala L. in traditional Iranian medicine and modern phytotherapy: a review. J Tradit Chin Med. 2015;35:104–9.
29. Moustafa NE, Alomari AA. Green synthesis and bactericidal activities of isotropic and anisotropic spherical gold nanoparticles produced using Peganum harmala L leaf and seed extracts. Biotechnol Appl Biochem. 2019;66:664–72.
30. Moloudizargari M, Mikaili P, Aghajanshakeri S, Asghari MH, Shayegh J. Pharmacological and therapeutic effects of Peganum harmala and its main alkaloids. Pharmacogn Rev. 2013;7:199–212.
31. Zhu Z, Zhao S, Wang C. β-Carboline alkaloids from Peganum harmala inhibit fusarium oxysporum from Codonopsis radix through damaging the cell membrane and inducing ROS accumulation. Pathogens. 2022;11:1341.
32. Di Giorgio C, Delmas F, Ollivier E, Elias R, Balansard G, Timon-David P. In vitro activity of the beta-carboline alkaloids Harmane, Harmine, and harmaline toward parasites of the species leishmania infantum. Exp Parasitol. 2004;106:67–74.
33. Chen B, Wu J, Yan Z, Wu H, Gao H, Liu Y, Zhao J, Wang J, Yang J, Zhang Y, Pan J, Ling Y, Wen H, Huang Z. 1,3-Substituted β-Carboline derivatives as potent chemotherapy for the treatment of cystic echinococcosis. J Med Chem. 2023;66:16680–93.
34. Perković I, Raić-Malić S, Fontinha D, Prudêncio M, Pessanha de Carvalho L, Held J, Tandarić T, Vianello R, Zorc B, Rajić Z. Harmicines - harmine and cinnamic acid hybrids as novel antiplasmodial hits. Eur J Med Chem. 2020;187:111927.
35. Poje G, Pessanha de Carvalho L, Held J, Moita D, Prudêncio M, Perković I, Tandarić T, Vianello R, Rajić Z. Design and synthesis of harmiquins, Harmine and chloroquine hybrids as potent antiplasmodial agents. Eur J Med Chem. 2022;238:114408.
36. Shahinas D, Macmullin G, Benedict C, Crandall I, Pillai DR. Harmine is a potent antimalarial targeting Hsp90 and synergizes with chloroquine and Artemisinin. Antimicrob Agents Chemother. 2012;56:4207–13.
37. Pavić K, Poje G, Pessanha de Carvalho L, Tandarić T, Marinović M, Fontinha D, Held J, Prudêncio M, Piantanida I, Vianello R, Krošl Knežević I, Perković I, Rajić Z. Discovery of Harmiprims, harmine-primaquine hybrids, as potent and selective anticancer and antimalarial compounds. Bioorg Med Chem. 2024;105:117734.
38. Cao R, Fan W, Guo L, Ma Q, Zhang G, Li J, Chen X, Ren Z, Qiu L. Synthesis and structure-activity relationships of Harmine derivatives as potential antitumor agents. Eur J Med Chem. 2013;60:135–43.
39. Hu D, Han G, Ren H, Li X, Li X, Yue L, Xu J, Feng J, Guo L. Synthesis, biological evaluation and preliminary mechanisms of 6-amino substituted Harmine derivatives as potential antitumor agents. Fitoterapia. 2022;163:105329.
40. Zhang XF, Sun RQ, Jia YF, Chen Q, Tu RF, Li KK, Zhang XD, Du RL, Cao RH. Synthesis and mechanisms of action of novel Harmine derivatives as potential antitumor agents. Sci Rep. 2016;6:33204.
41. Costa-Machado LF, Garcia-Dominguez E, McIntyre RL, Lopez-Aceituno JL, Ballesteros-Gonzalez Á, Tapia-Gonzalez A, Fabregat-Safont D, Eisenberg T, Gomez J, Plaza A, Sierra-Ramirez A, Perez M, Villanueva-Bermejo D, Fornari T, Loza MI, Herradon G, Hofer SJ, Magnes C, Madeo F, Duerr JS, Pozo OJ, Galindo MI, Del Pino I, Houtkooper RH, Megias D, Viña J, Gomez-Cabrera MC, Fernandez-Marcos PJ. Peripheral modulation of antidepressant targets MAO-B and GABAAR by Harmol induces mitohormesis and delays aging in preclinical models. Nat Commun. 2023;14:2779.
42. Fortunato JJ, Réus GZ, Kirsch TR, Stringari RB, Fries GR, Kapczinski F, Hallak JE, Zuardi AW, Crippa JA, Quevedo J. Chronic administration of Harmine elicits antidepressant-like effects and increases BDNF levels in rat hippocampus. J Neural Transm (Vienna). 2010;117:1131–7.
43. Liu F, Wu J, Gong Y, Wang P, Zhu L, Tong L, Chen X, Ling Y, Huang C. Harmine produces antidepressant-like effects via restoration of astrocytic functions. Prog Neuropsychopharmacol Biol Psychiatry. 2017;79:258–67.
44. Xie Z, Liu W, Dang R, Hu X, Cai F, Xiang Z, Zhao X, Cheng X, Wang C. Effects and mechanisms of Harmine on ameliorating ethanol-induced memory impairment. J Ethnopharmacol. 2025;337:118789.
45. Rosselot C, Li Y, Wang P, Alvarsson A, Beliard K, Lu G, Kang R, Li R, Liu H, Gillespie V, Tzavaras N, Kumar K, DeVita RJ, Stewart AF, Stanley SA. Garcia-Ocaña A. Harmine and exendin-4 combination therapy safely expands human B cell mass in vivo in a mouse xenograft system. Sci Transl Med. 2024;16:eadg3456.
46. Lu S, Wen L, Gong Y, Tian C, Gao H, Chen B, Lü G, Zhao J, Wang J. In vitro effects of Harmine against Echinococcus granulosus Protoscoleces by stimulating DNA damage. Exp Parasitol. 2021;226–227:108121.
47. Khan H, Patel S, Kamal MA. Pharmacological and toxicological profile of Harmane-β-Carboline alkaloid: friend or foe. Curr Drug Metab. 2017;18:853–7.
48. Gao HJ, Teng L, Zhao J, Wang JH, Ran X, Xu N, Gong YH, Wen LM, Wang BJ, Chen B. The pharmacokinetics and tissue distribution of Harmine derivative H-2-104 in rats. J Biol Regul Homeost Agents. 2022;36:2069–84.

49. Eylem CC, Yilmaz M, Derkus B, Nemutlu E, Camci CB, Yilmaz E, Turkoglu MA, Aytac B, Ozyurt N, Emregul E. Untargeted multi-omic analysis of colorectal cancer-specific exosomes reveals joint pathways of colorectal cancer in both clinical samples and cell culture. Cancer Lett. 2020;469:186–94.
50. Gonulalan EM, Nemutlu E, Bayazeid O, Koçak E, Yalçın FN, Demirezer LO. Metabolomics and proteomics profiles of some medicinal plants and correlation with BDNF activity. Phytomedicine. 2020;74:152920.
51. Johnson CH, Ivanisevic J, Siuzdak G. Metabolomics: beyond biomarkers and towards mechanisms. Nat Rev Mol Cell Biol. 2016;17:451–9.
52. Gong Y, Lv S, Tian C, Gao Y, Chen B, Wen L, Gao H, Aimaiti W, Ma R, Zhao J, Wang J. Effect of Harmine and its derivatives against Echinococcus granulosus and comparison of DNA damage targets. J Biomed Nanotechnol. 2020;16:827–41.
53. Buschmann J. The OECD guidelines for the testing of chemicals and pesticides. Methods Mol Biol. 2013;947:37–56.
54. Kandil A, Keles AG, Balci H, Demirci Tansel C. The effects of nitric oxide and inhibitor, and combination of albendazole and praziquantel on liver in mice injected with Echinococcus granulosus larvae. Acta Trop. 2021;219:105917.
55. Wishart DS, Guo A, Oler E, Wang F, Anjum A, Peters H, Dizon R, Sayeeda Z, Tian S, Lee BL, Berjanskii M, Mah R, Yamamoto M, Jovel J, Torres-Calzada C, Hiebert-Giesbrecht M, Lui VW, Varshavi D, Varshavi D, Allen D, Arndt D, Khetarpal N, Sivakumaran A, Harford K, Sanford S, Yee K, Cao X, Budinski Z, Liigand J, Zhang L, Zheng J, Mandal R, Karu N, Dambrova M, Schiöth HB, Greiner R, Gautam V. HMDB 5.0: the human metabolome database for 2022. Nucleic Acids Res. 2022;50:D622–31.
56. Horai H, Arita M, Kanaya S, Nihei Y, Ikeda T, Suwa K, Ojima Y, Tanaka K, Tanaka S, Aoshima K, Oda Y, Kakazu Y, Kusano M, Tohge T, Matsuda F, Sawada Y, Hirai MY, Nakanishi H, Ikeda K, Akimoto N, Maoka T, Takahashi H, Ara T, Sakurai N, Suzuki H, Shibata D, Neumann S, Iida T, Tanaka K, Funatsu K, Matsuura F, Soga T, Taguchi R, Saito K, Nishioka T. MassBank: a public repository for sharing mass spectral data for life sciences. J Mass Spectrom. 2010;45:703–14.
57. Wixon J, Kell D. The Kyoto encyclopedia of genes and genomes–KEGG. Yeast. 2000;17:48–55.
58. Sud M, Fahy E, Cotter D, Brown A, Dennis EA, Glass CK, Merrill AH Jr., Murphy RC, Raetz CR, Russell DW, Subramaniam S. LMSD: LIPID MAPS structure database. Nucleic Acids Res. 2007;35:D527–532.
59. Abdelrazig S, Safo L, Rance GA, Fay MW, Theodosiou E, Topham PD, Kim DH, Fernández-Castané A. Metabolic characterisation of Magnetospirillum gryphiswaldense MSR-1 using LC-MS-based metabolite profiling. RSC Adv. 2020;10:32548–60.
60. Thévenot EA, Roux A, Xu Y, Ezan E, Junot C. Analysis of the human adult urinary metabolome variations with age, body mass index, and gender by implementing a comprehensive workflow for univariate and OPLS statistical analyses. J Proteome Res. 2015;14:3322–35.
61. Xia J, Wishart DS. Web-based inference of biological patterns, functions and pathways from metabolomic data using metaboanalyst. Nat Protoc. 2011;6:743–60.
62. Chen B, Yan M, Gao H, Ma Q, Li L, Lü G, Gong Y, Wen L, Xu S, Wang J, Zhao J. In vitro and in vivo efficacies of novel harmine derivatives in the treatment of cystic echinococcosis. Drug Des Devel Ther. 2023;17:2441–54.
63. Bakhtiar NM, Spotin A, Mahami-Oskouei M, Ahmadpour E, Rostami A. Recent advances on innate immune pathways related to host-parasite cross-talk in cystic and alveolar echinococcosis. Parasit Vectors. 2020;13:232.
64. Mohammed S, Thadathil N, Selvarani R, Nicklas EH, Wang D, Miller BF, Richardson A, Deepa SS. Necroptosis contributes to chronic inflammation and fibrosis in aging liver. Aging Cell. 2021;20:e13512.
65. Schwabe RF, Luedde T. Apoptosis and necroptosis in the liver: a matter of life and death. Nat Rev Gastroenterol Hepatol. 2018;15:738–52.
66. Vucur M, Ghallab A, Schneider AT, Adili A, Cheng M, Castoldi M, Singer MT, Büttner V, Keysberg LS, Küsgens L, Kohlhepp M, Görg B, Gallage S, Barragan Avila JE, Unger K, Kordes C, Leblond AL, Albrecht W, Loosen SH, Lohr C, Jördens MS, Babler A, Hayat S, Schumacher D, Koenen MT, Govaere O, Boekschoten MV, Jörs S, Villacorta-Martin C, Mazzaferro V, Llovet JM, Weiskirchen R, Kather JN, Starlinger P, Trauner M, Luedde M, Heij LR, Neumann UP, Keitel V, Bode JG, Schneider RK, Tacke F, Levkau B, Lammers T, Fluegen G, Alexandrov T, Collins AL, Nelson G, Oakley F, Mann DA, Roderburg C, Longerich T, Weber A, Villanueva A, Samson AL, Murphy JM, Kramann R, Geisler F, Costa IG, Hengstler JG, Heikenwalder M, Luedde T. Sublethal necroptosis signaling promotes inflammation and liver cancer. Immunity. 2023;56:1578–e15951578.
67. Kisseleva T, Brenner D. Molecular and cellular mechanisms of liver fibrosis and its regression. Nat Rev Gastroenterol Hepatol. 2021;18:151–66.
68. Xu S, Chen Y, Miao J, Li Y, Liu J, Zhang J, Liang J, Chen S, Hou S. Esculin inhibits hepatic stellate cell activation and CCl(4)-induced liver fibrosis by activating the Nrf2/GPX4 signaling pathway. Phytomedicine. 2024;128:155465.
69. Ma Y, Li W, Yao Q, Liu Y, Yu J, Zang L, Wang S, Zhou L, Wen S, Luo Y, Li W, Niu X. Harmine ameliorates CCl(4)-induced acute liver injury through suppression of autophagy and inflammation. Int Immunopharmacol. 2024;129:111538.
70. Kagan VE, Mao G, Qu F, Angeli JP, Doll S, Croix CS, Dar HH, Liu B, Tyurin VA, Ritov VB, Kapralov AA, Amoscato AA, Jiang J, Anthonymuthu T, Mohammadyani D, Yang Q, Proneth B, Klein-Seetharaman J, Watkins S, Bahar I, Greenberger J, Mallampalli RK, Stockwell BR, Tyurina YY, Conrad M, Bayır H. Oxidized arachidonic and adrenic PEs navigate cells to ferroptosis. Nat Chem Biol. 2017;13:81–90.
71. Lee DK, Choi KH, Oh JN, Kim SH, Lee M, Jeong J, Choe GC, Lee CK. Linoleic acid reduces apoptosis via NF-κB during the in vitro development of induced parthenogenic Porcine embryos. Theriogenology. 2022;187:173–81.
72. Kasahara N, Imi Y, Amano R, Shinohara M, Okada K, Hosokawa Y, Imamori M, Tomimoto C, Kunisawa J, Kishino S, Ogawa J, Ogawa W, Hosooka T. A gut microbial metabolite of Linoleic acid ameliorates liver fibrosis by inhibiting TGF-β signaling in hepatic stellate cells. Sci Rep. 2023;13:18983.
73. Schuster S, Johnson CD, Hennebelle M, Holtmann T, Taha AY, Kirpich IA, Eguchi A, Ramsden CE, Papouchado BG, McClain CJ, Feldstein AE. Oxidized Linoleic acid metabolites induce liver mitochondrial dysfunction, apoptosis, and NLRP3 activation in mice. J Lipid Res. 2018;59:1597–609.
74. Tessari P, Vettore M, Millioni R, Puricelli L, Orlando R. Effect of liver cirrhosis on phenylalanine and tyrosine metabolism. Curr Opin Clin Nutr Metab Care. 2010;13:81–6.
75. She H, Du Y, Du Y, Tan L, Yang S, Luo X, Li Q, Xiang X, Lu H, Hu Y, Liu L, Li T. Metabolomics and machine learning approaches for diagnostic and prognostic biomarkers screening in sepsis. BMC Anesthesiol. 2023;23:367.
76. Zhu M, Du X, Xu H, Yang S, Wang C, Zhu Y, Zhang T, Zhao W. Metabolic profiling of liver and faeces in mice infected with echinococcosis. Parasit Vectors. 2021;14:324.
77. Brown DG, Rao S, Weir TL, O'Malia J, Bazan M, Brown RJ, Ryan EP. Metabolomics and metabolic pathway networks from human colorectal cancers, adjacent mucosa, and stool. Cancer Metab. 2016;4:11.
78. Drury J, Geisen ME, Tessmann JW, Rychahou PG, Kelson CO, He D, Wang C, Evers BM, Zaytseva YY. Overexpression of fatty acid synthase upregulates Glutamine-Fructose-6-Phosphate transaminase 1 and O-Linked N-Acetylglucosamine transferase to increase O-GlcNAc protein glycosylation and promote colorectal Cancer growth. Int J Mol Sci. 2024;25:4883.
79. Feng Y, Xu J, Lu J, Hou J, Wang L, Dong D, Wang X, Wang X, Wu X, Chen X. EgCF mediates macrophage polarisation by influencing the glycolytic pathway. J Helminthol. 2023;97:e101.
80. Tian T, Mao Q, Xie J, Wang Y, Shao WH, Zhong Q, Chen JJ. Multi-omics data reveals the disturbance of glycerophospholipid metabolism caused by disordered gut microbiota in depressed mice. J Adv Res. 2022;39:135–45.
81. Zheng P, Wu J, Zhang H, Perry SW, Yin B, Tan X, Chai T, Liang W, Huang Y, Li Y, Duan J, Wong ML, Licinio J, Xie P. The gut Microbiome modulates gut-brain axis glycerophospholipid metabolism in a region-specific manner in a non-human primate model of depression. Mol Psychiatry. 2021;26:2380–92.

Publisher's note